Chinese Physics B

PAPER

Accurate electron affinity of atomic cerium and excited states of its anion*

Accurate electron affinity of atomic cerium and excited states of its anion*

Xiao-Xi Fu(付筱茜)[1], Ru-Lin Tang(唐如麟)[1], Yu-Zhu Lu(陆禹竹)[1], and Chuan-Gang Ning(宁传刚)[1,2,†]

[1] *Department of Physics, State Key Laboratory of Low-Dimensional Quantum Physics, Tsinghua University, Beijing* 100084, *China*
[2] *Collaborative Innovation Center of Quantum Matter, Beijing* 100084, *China*

(Received 7 April 2020; revised manuscript received 29 April 2020; accepted manuscript online 7 May 2020)

Electron affinities (EA) of most lanthanide elements still remain unknown owing to their relatively lower EA values and the fairly complicated electronic structures. In the present work, we report the high-resolution photoelectron spectra of atomic cerium anion Ce^- using the slow electron velocity-map imaging method in combination with a cold ion trap. The electron affinity of Ce is determined to be 4840.62(21) cm^{-1} or 0.600160(26) eV. Moreover, several excited states of Ce^- ($^4H_{9/2}$, $^4I_{9/2}$, $^2H_{9/2}$, $^2G_{9/2}$, $^2G_{7/2}$, $^4H_{13/2}$, $^2F_{5/2}$, and $^4I_{13/2}$) are observed.

Keywords: electron affinity, cerium anion, slow electron velocity-map imaging, cold ion trap

PACS: 32.10.Hq, 32.80.Gc, 37.10.Rs, 37.10.Ty **DOI:** 10.1088/1674-1056/ab90e9

1. Introduction

Negative ions have rendered us a better understanding of electron correlation effects and dynamics in atomic and molecular systems. The extra electron is weakly bound to the neutral core by correlation effects and the polarization of the atomic charge cloud produced by itself. The resultant short-range potential generally tends to support only one bound state. As a sharp contrast, the long-range Coulomb forces peculiar to atoms or positive ions bring about infinite bound states. However, strong electron correlation effects do allow the existence of a few bound excited states of some atomic lanthanide anions. For example, La^- [1,2] and Ce^- [1] possess 15 and 32 bound states, respectively. In particular, it has been confirmed experimentally that La^-,[3,4] Ce^-,[5,6] Os^-,[7,8] and Th^- [9,10] even have bound states with opposite parities. This is the prerequisite for laser cooling as a strong electric dipole cycling transition is needed.[11–14]

The electronic configuration of the ground state of Ce atom is [Xe]4f5d6s^2. The strong correlation effects caused by the unusual chemical bonding of 4f electrons of Ce atoms turn many Ce compounds into strongly correlated materials.[15,16] Furthermore, the intertwined magnetic and Kondo physics of Ce-based compounds has made Ce-system an ideal platform to study the interplay between magnetism, Kondo effects, superconductivity, and multiple quantum phase transitions.[17,18] To explore the abundant physics of Ce-system, it is of fundamentally physical importance to study the properties of Ce. Unfortunately, the complicated electronic structures make most of the atomic lanthanide anions including Ce^- remain unexplored thoroughly. The partially filled f- and d-subshells make the conventional quantum computational method fail to take all the tricky correlation effects into account. In other words, it is imperative to acquire fundamental parameters such as electron affinity experimentally so as to compare these results with the calculated ones to modify the theoretical models.

Electron affinity (EA) is defined as the energy difference between the ground states of the negative ion and the neutral system. It can be regarded as the energy needed to remove the extra electron from the negative ion or the energy released when the extra electron is added to the neutral system. EA reflects the ability of an atom to accept an electron. In contrast to EA, ionization potential (IP) describes the ability of an atom to lose an electron. The IPs of elements with atomic number $Z \leqslant 119$ have been investigated systematically and thoroughly.[19] However, EAs are hard to predict with a relatively small error. As a result, various sophisticated techniques have been developed so far such as hyperspherical calculations for Li^- and Na^- [20] and coupled-cluster method for S_3.[21] These accurate values of lighter elements or simple compounds are in excellent agreement with experimental data. On the part of complicated systems with increased number of electrons like lanthanide elements, the calculated results are far away from satisfactory due to the tricky electron correlation effects and relativistic effects.[22] The latest progress and research status of EA of Ce are summarized as follows. Dinov *et al.*[23] applied valence-shell relativistic configuration-interaction calculations and obtained electron affinity of Ce to be 0.259 eV. Later they revised their result to be 0.428 eV[24] through better treatment of the second order effect and a more appropriate choice of neutral threshold. Berkovits *et al.*[25] determined an adiabatic electron affinity to be 0.70(1) eV through observed detachment thresholds which were attributed to transitions detached

*Project supported by the National Natural Science Foundation of China (Grant Nos. 91736102 and 11974199) and the National Key R&D Program of China (Grant No. 2018YFA0306504).

†Corresponding author. E-mail: ningcg@tsinghua.edu.cn

to neutral excited states. Davis and Thompson[26] measured the electron affinity of cerium to be 0.955(26) eV using laser photodetachment electron spectroscopy. Cao and Dolg[27] adopted relativistic energy-consistent small-core pseudopotential methodology and reported the result to be 0.58(10) eV considering the averaged coupled pair functional-type corrections to the multireference configuration-interaction value as well as possible finite basis set errors. By considering correlation involving core electrons, O'Malley and Beck revised the EA of Ce as 0.660 eV[28] via reinterpreting Davis and Thompson's spectra. Felfli *et al.*[29] applied Regge-pole methodology for electron–atom elastic scattering and predicted the EA to be 0.61 eV. Walter *et al.*[5] investigated the negative ion of Ce using tunable laser photodetachment threshold spectroscopy and obtained the EA of Ce to be 0.65(3) eV. Later, Walter *et al.*[6] conducted experimental study with tunable infrared laser photodetachment spectroscopy and theoretical study with relativistic configuration interaction in the continuum formalism. Through identification of resonance spectrum by theoretic calculations of photodetachment cross sections, the EA was determined to be 0.628(10) eV. Recently, Felton *et al.*[30] measured the EA to be 0.570(20) eV through photoelectron energy spectroscopy.

In this work, we employed slow electron velocity-map imaging (SEVI) method combined with a cryogenically controlled ion trap to conduct the measurement of EA of cerium atom and the excited states of cerium anion. To test the performance of this spectrometer, we compared our measured results of two main group elements, i.e., I and S,[31] with those obtained via the laser photodetachment microscopy (LPM) method by Blondel and co-workers.[32,33] Our data are in agreement with the LPM results. For the photoelectron spectrum of S^-,[31] the energy resolution [the full width at half maximum (FWHM)] is 0.53 cm^{-1} for the peak with the electron kinetic energy $E_k = 1.08$ cm^{-1} at an imaging voltage of -150 V. We determined the EA value of S to be 16753.00(7) cm^{-1}, in an excellent agreement with the LPM result (16752.9753(41) cm^{-1}).[33] The SEVI method has demonstrated an excellent energy resolution for slow electrons, typically a few cm^{-1} near the photodetachment threshold, which is an essential feature for resolving the congested photoelectron spectra of Ce^-. Using this method, we have already determined the EA values of several main group elements, transition elements, and lanthanides with an accuracy 0.1–1 cm^{-1}.[31,34–40] Our experimental setup is described in Section 2. Then we discuss the way we assigned the photoelectron spectra of Ce^- in Subsection 3.1, followed by the accurate measurement of EA of cerium in Subsection 3.2, as well as the optimized binding energies gained through global optimization analysis in Subsection 3.3. Finally, we summarize our experimental results in Section 4.

2. Experimental setup

Our apparatus has been described in detail previously.[36,40] Briefly, negative Ce ions are produced when ablation laser is focused on the surface of a cerium metal disk which is rotating and translating at the same time. Then the negative ions fly into an ion trap, which is mounted on a cryogenically controlled cold head with a variable temperature 5–300 K. While being trapped in the ion trap, the ions tend to lose kinetic energies in the process of collisions with buffer gas which is the mixture of 20% H_2 and 80% He. After being trapped for 45 ms, the ions are thrown out via the pulsed potentials on the end caps of the trap. The ion trap can be turned off so that the ions can directly fly through the ion trap. Under this mode, excited states with short lifetimes can have more chances to be detected. Then they are accelerated by a -1000 V high-voltage pulse in the Wiley–McLaren time-of-flight mass spectrometer,[41] and finally detected by a microchannel-plate (MCP) type detector. The ion detector can be moved out of the ion path during the photodetachment phase. The ions of interest are chosen out via a mass gate, and are photodetached by tunable dye laser (linearly polarized, 400–920 nm, linewidth 0.06 cm^{-1} at 625 nm) in the interaction area of the imaging lens.[42,43] A HighFinesse WS-600 wavelength meter with an accuracy of 0.02 cm^{-1} monitors the wavelength of the dye laser in real time. The outgoing photoelectrons are projected onto a microchannel-plate enhanced phosphor screen. The hitting position of each photoelectron is recorded in an event-counting mode by a charge-coupled device (CCD) camera in real time. Each raw photoelectron image is usually an accumulated result of 50000 laser shots. The photoelectrons with the same kinetic energy will form a spherical shell before hitting on the phosphor screen. The radius r of the spherical shell is proportional to the velocity of the electrons. The spherical shells of the photoelectrons have cylindrical symmetry. Therefore, three-dimensional (3D) distributions can be reconstructed from the projected two-dimensional (2D) images. The maximum-entropy velocity Lengendre method is applied in this work to reconstruct the radial and angular distributions.[44]

3. Results and discussion

3.1. Assignments of the photoelectron energy spectra

Figure 1 shows the photoelectron energy spectra of Ce^- at the photon energy $h\nu = 11595$ cm^{-1}. In order to distinguish transitions with different initial states, the spectra were plotted together under two different working modes. More peaks were observed when the ion trap was turned off. These extra peaks are related to the short-lived excited states. In the trap-off mode, the Ce^- ions took about 0.4 ms to fly from the ion source to the photodetachment zone. Apparently, a peak from an excited anionic state will become weaker when the

ion trap is turned on if its lifetime is comparable to the trapping time 45 ms. And, if two peaks share the same initial state, the changing trend of the intensities should be identical. In view of the previously experimental EA results, the changing trends and the known energy levels of the neutral Ce atom with a high accuracy, there is no doubt that peaks 6, 8, 16, and 27 are from the anionic ground state $^4H_{7/2}$. As shown in Fig. 1, there still exists some overlapped peaks due to the dense photodetachment channels. To further confirm the assignment, methane (CH_4) gas, which can de-excite metastable states more effectively since it has more internal states,[45] was further introduced as the buffer gas in the ion trap. As demonstrated in Fig. 2, peaks 4, 5, 11, and 19 disappear, and peaks 9 and 21 fall sharply, which implies that these peaks originate from different excited states. Peak 6, which does not manifest any variation, can be assigned with certainty to the photodetachment channel from the ground state of the anion Ce^- to the ground state of the neutral Ce atom. Based on the changing trends of the peak intensities as the experimental conditions alter, the simulated photoelectron energy spectra by Beck,[28] and the energy levels of neutral Ce atom,[46] the assigned photodetachment channels are visually summarized in the bottom part of Fig. 1. The relative energy positions of anionic states $^4H_{7/2}$, $^4H_{9/2}$, and $^4I_{9/2}$ determined through the infrared resonant photodetachment spectroscopy[6] are conducive to assignning some weak peaks in Fig. 1. The relative positions of the sticks under the spectra are locked in line with the energy levels of the neutral atom Ce if these channels derive from a common anionic state. The black and green sticks refer to channels photodetached from the ground state $^4H^o_{7/2}$ of Ce^- and the excited states of Ce^- labelled on the left or right sides, respectively.

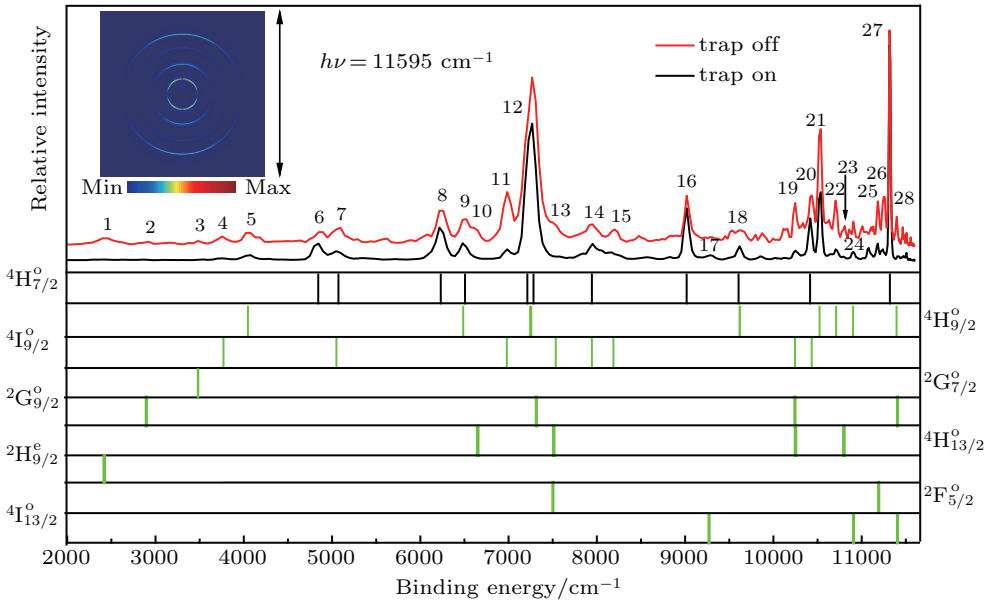

Fig. 1. Comparison of photoelectron energy spectra of Ce^- in the ion-trap-off mode (the upper red line) and in the ion-trap-on mode (the lower black line). In the ion-trap-on mode, Ce^- ions are trapped for 45 ms with the buffer gas H_2+He. The ion trap can be turned off to observe excited states with short lifetimes. The sets of sticks below the spectra indicate the energy levels of the final neutral states of photodetachment channels from the same anionic states labeled on the left or right sides. The black sticks are for the anionic ground state, and green for the excited states. The inset shows the photoelectron image obtained under the trap-on mode. The double arrow corresponds to the polarization of the photodetachment laser.

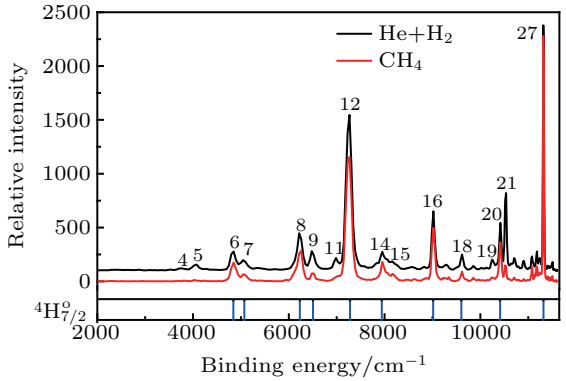

Fig. 2. Photoelectron spectra of Ce^- obtained with H_2+He buffer gas (the upper black line) and CH_4 buffer gas (the lower red line). The vertical sticks indicate the energy levels of final states of photodetachment channels from the ground state $^4H_{7/2}$ of Ce^-.

3.2. Accurate measurement of the EA of cerium

Since the energy levels of the neutral atom Ce are well known with a high accuracy,[46] any peak from the anionic ground state can be chosen to determine the EA value of Ce atom. In the present work, the strong peak labeled 27 is selected to measure the EA value since its binding energy (BE) lies within the tuning range of our dye laser. The transition of peak 27 is $Ce(^3H_4) \leftarrow Ce^-(^4H_{7/2})$. To accurately measure the binding energy of peak 27, we scanned the photon energy slightly above the photodetachment threshold of this peak from 11348 cm^{-1} to 11428 cm^{-1} with a step of 20 cm^{-1} at the imaging voltage −300 V. Since the ejected photoelectrons with the same kinetic energy form a spherical shell and

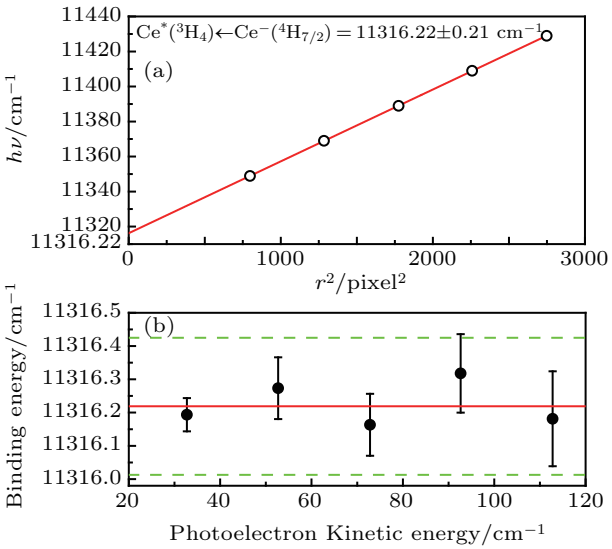

Fig. 3. (a) The photon energy $h\nu$ versus r^2 for transition 27. The solid line is the linear least square fitting. The intercept 11316.22 cm^{-1} is the binding energy of transition 27. (b) The binding energy of transition $Ce(^3H_4) \leftarrow Ce^-(^4H_{7/2})$ as a function of the kinetic energy of photoelectrons. The dashed lines indicate the uncertainty ± 0.21 cm^{-1}.

are projected onto the screen as a ring, the radius r of the ring is proportional to the velocity of the photoelectrons. As shown in Fig. 3, the experimental data plotted as $h\nu$ versus r^2 form a line. The binding energy of peak 27 is equivalent to the intercept of the fitted line with the $h\nu$-axis in virtue of the relation $h\nu = BE + \alpha r^2$, where α is a coefficient. Thus, the binding energy of transition $Ce(^3H_4) \leftarrow Ce^-(^4H_{7/2})$ is determined to be 11316.22±0.21 cm^{-1}. By subtracting the energy level 6475.540 cm^{-1} [46] of the final state $^3H_4$, the EA value of Ce is determined to be 4840.68(21) cm^{-1}. The uncertainty has included the laser linewidth of 0.06 cm^{-1}.

3.3. Optimized BEs through a global optimization analysis

There are multiple transition energies measured for each initial state. In order to make use of the wealth of information we have accumulated, a global optimization analysis based on covariance algebra was conducted to obtain the interval between any two energy levels.[47–49] The measured values including the uncertainties obtained in this work, the energy levels of neutral Ce, and the energy intervals of anionic states $^4H_{7/2}$, $^4H_{9/2}$, and $^4I_{9/2}$ [6] were used as input information for the consistent analysis. By subtracting the energy level 6475.540 cm^{-1} [46] of the final state $^3H_4$ from the optimized value 11316.16±0.21 cm^{-1}, the optimized EA

Table 1. Measured binding energies and optimized binding energies of the transitions observed in this present work.

Peaks	Levels (Ce ← Ce$^-$)	Measured binding energy/cm^{-1}	Optimized binding energy/cm^{-1}
1	$^1G_4 \leftarrow ^2 H_{9/2}$	2439(100)	2439(100)
2	$^1G_4 \leftarrow ^2 G_{9/2}$	2897(120)	2887(2)
3	$^1G_4 \leftarrow ^2 G_{7/2}$	3486(88)	3486(88)
4	$^1G_4 \leftarrow ^4 I_{9/2}$	3752(86)	3758(6)
5	$^1G_4 \leftarrow ^4 H_{9/2}$	4054(76)	4052.61(38)
6	$^1G_4 \leftarrow ^4 H_{7/2}$	4840(64)	4841.16(21)
7	$^3F_2 \leftarrow ^4 H_{7/2}/^3H_4 \leftarrow ^4 I_{9/2}$	5069(60)	5070.16(22)/5037(6)
8	$^3G_3 \leftarrow ^4 H_{7/2}$	6241(46)	6230.16(22)
9	$^3F_3 \leftarrow ^4 H_{7/2}/^5H_4 \leftarrow ^4 H_{9/2}$	6504(42)	6504.16(22)/6490.61(38)
10	$^5I_6 \leftarrow ^4 H_{13/2}$	6628(42)	6649(7)
11	$^3G_5 \leftarrow ^4 I_{9/2}$	6988(38)	6968(6)
12	$^5H_4 \leftarrow ^4 H_{7/2}/^3G_5 \leftarrow ^4 H_{9/2}/^5I_4 \leftarrow ^4 H_{9/2}/^5H_3 \leftarrow ^4H_{7/2}/^3G_5 \leftarrow ^2G_{9/2}$	7263(120)	7210.16(22)/7249.61(38)/7262.61(38) /7279.16(22)/7305(2)
13	$^5I_7 \leftarrow ^4 H_{13/2}/^5D_2 \leftarrow ^2 F_{5/2}/^5I_5 \leftarrow ^4 I_{9/2}$	7497(170)	7509(7)/7487(3)/7522(6)
14	$^3F_4 \leftarrow ^4 H_{7/2}/^3G_4 \leftarrow ^4 I_{9/2}$	7934(32)	7941.16(22)/7931(6)
15	$^3G_5 \leftarrow ^4 I_{9/2}$	8196(28)	8175(6)
16	$^3G_4 \leftarrow ^4 H_{7/2}$	9016(18)	9014.16(22)
17	$^3I_6 \leftarrow ^4 I_{13/2}$	9265(140)	9263(2)
18	$^3H_4 \leftarrow ^4 H_{7/2}/^5D_4 \leftarrow ^4 H_{9/2}$	9615(14)	9604.16(22)/9624.61(38)
19	$^5G_6 \leftarrow ^4 H_{13/2}/^1G_4 \leftarrow ^2 G_{9/2}/^3H_4 \leftarrow ^4 I_{9/2}$	10245(14)	10248(7)/10235(2)/10233(6)
20	$^5D_4 \leftarrow ^4 H_{7/2}/^3I_5 \leftarrow ^4 I_{9/2}$	10417(8)	10413.16(22)/10421(6)
21	$^3H_4 \leftarrow ^4 H_{9/2}$	10528(7)	10527.61(37)
22	$^3I_5 \leftarrow ^4 H_{9/2}$	10711(9)	10715.61(38)
23	$^5G_6 \leftarrow ^4 H_{13/2}$	10798(8)	10796(7)
24	$^3I_6 \leftarrow ^4 I_{13/2}/^5G_4 \leftarrow ^4 H_{9/2}$	10904(5)	10900(2)/10908.61(38)
25	$^1F_3 \leftarrow ^2 F_{5/2}$	11179(3)	11179(3)
26		11234(6)	
27	$^3H_4 \leftarrow ^4 H_{7/2}$	11316.22(21)	11316.16(21)
28	$^1G_4 \leftarrow ^4 H_{9/2}/^1I_6 \leftarrow ^4 I_{13/2}/^3H_4 \leftarrow ^2 G_{9/2}$	11396(2)	11400.60(38)/11397(2)/ 11396(2)

Table 2. The previously reported electron affinity values of Ce in comparison with this work.

Value/eV	Reference
0.259	Dinov *et al.* (calculated)[23]
0.428	O'Malley and Beck (calculated)[24]
0.660	O'Malley and Beck (calculated)[28]
0.61	Felfli *et al.*(calculated)[29]
0.58(10)	Cao and Dolg (calculated)[27]
0.700(10)	Berkovits *et al.* (measured)[25]
0.955(26)	Davis and Thompson (measured)[26]
0.65(3)	Walter *et al.*(measured)[5]
0.628(10)	Walter *et al.*(measured)[6]
0.570(20)	Felton *et al.*(measured)[30]
0.600160(26)	this work

value of Ce is 4840.62(21) cm^{-1} or 0.600160(26) eV. Note that 1 eV = 8065.543937$\cdots$ cm^{-1}, as recommended by 2018 CODATA.[50] It is worth mentioning that our present EA value is less than the energies of even-parity ($4f5d6s^26p$) states $^2H_{9/2}$ and $^2F_{7/2}$ of Ce^- obtained via the infrared absorption spectroscopy by Walter *et al.*[6] This means that peak *A* with a resonant energy 0.61816(3) eV and peak *u* with a resonant energy 0.60023(3) eV[6] are not bound-to-bound transitions. Moreover, the energy level 1159(40) cm^{-1} of $^4I^o_{9/2}$ determined by Walter *et al.*[6] is not consistent with our value 1083(6) cm^{-1}. The reason is not clear. It is either due to the low signal-to-noise ratio of the broad peak *r*[6] or due to possible multiple resonances. The measured binding energies and the optimized ones of the assigned peaks are listed in Table 1. Our measured EA value is also compared with the previously reported values in Table 2. Table 3 summarizes the optimized energy levels of the bound states of Ce^-.

Table 3. The relative optimized energy levels of bound states of Ce^- (cm^{-1}).

State		Theory [28]	Theory [27]	Experiment [6][a]	This work
$4f5d^26s^2$	$^4H^o_{7/2}$	0	0	0	0
	$^4H^o_{9/2}$	887	879	788.41(32)	788.56(31)
	$^4I^o_{9/2}$	1226	2323	1159(40)	1083(6)
	$^2G^o_{7/2}$	1871	1597		1355(88)
	$^4H^o_{11/2}$	1944	2427		
	$^2G^o_{9/2}$	2073	2048		1954(2)
	$^4H^o_{13/2}$	2885	3597		2648(7)
	$^4D^o_{1/2}$	2888			
	$^2F^o_{5/2}$	3436	2919		2564(3)
	$^2F^o_{7/2}$	3452	3500		
	$^4D^o_{3/2}$	3460			
	$^4I^o_{13/2}$	3549			3274(2)
	$^2H^o_{9/2}$	4307			
	$^4D^o_{5/2}$	4315	4129		
	$^4F^o_{3/2}$	4468	3774		
	$^4I^o_{15/2}$	4630			
	$^2S^o_{1/2}$	4734			
	$^4F^o_{5/2}$	4887			
$4f5d6s^26p$	$^2H^e_{9/2}$	2904	3016		2402(100)
	$^2G^e_{7/2}$	3831	4210		
	$^4G^e_{5/2}$	4065	3629		
	$^2D^e_{3/2}$	4186			
	$^4H^e_{7/2}$	4654			
	$^2H^e_{11/2}$	4710			
	$^4I^e_{9/2}$	4960			

[a] The states $^2H_{9/2}$ and $^2F_{7/2}$ of Ce^- observed in Ref. [6] are not bound states.

4. Summary

The electron affinity of cerium is determined to be 4840.62(21) cm^{-1} or 0.600160(26) eV by using the SEVI method combined with a cold ion trap. Photoelectron spectra when the ion trap is on and off are accumulated and sketched together for better comparisons. Buffer gas is also altered from the mixture of helium and hydrogen to methane gas so as to de-excite metastable states more effectively. Besides, the energy levels of anionic states $^4H_{9/2}$, $^4I_{9/2}$, $^2H_{9/2}$, $^2G_{9/2}$, $^2G_{7/2}$, $^4H_{13/2}$, $^2F_{5/2}$, and $^4I_{13/2}$ are measured and optimized through a global optimization analysis.

Appendix A: Energy levels of Ce and Ce^- related to the present measurement

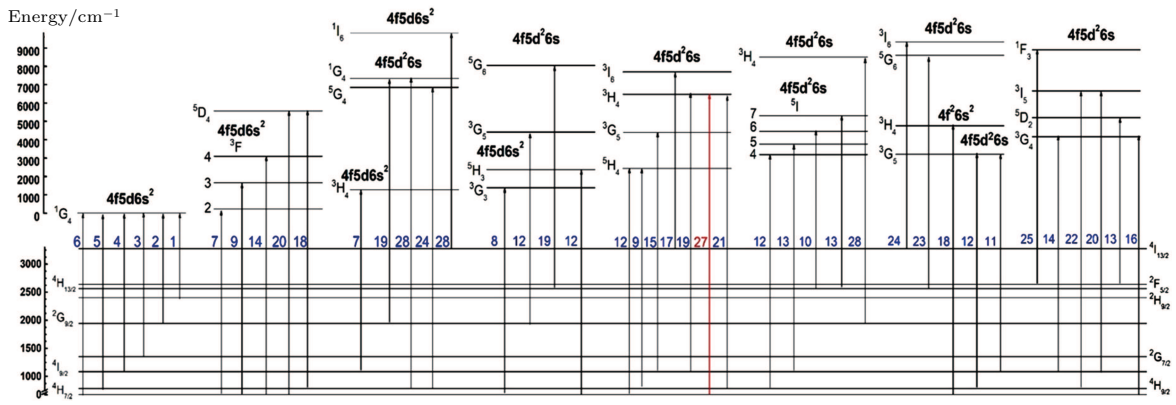

Fig. A1. Energy levels of Ce and Ce^- related to the present measurement. The ground state of Ce^- is $(4f5d^26s^2)^4H_{7/2}$. The ground state of Ce is $(4f5d6s^2)^1G_4$. The labels of each transition are the indexes of the observed peaks in Fig. 1. The transition 27 is used for the electron affinity measurement.

References

[1] O'Malley S M and Beck D R 2009 *Phys. Rev. A* **79** 012511
[2] Pan L and Beck D R 2016 *Phys. Rev. A* **93** 062501
[3] Pan L and Beck D R 2010 *Phys. Rev. A* **82** 014501
[4] Walter C W, Gibson N D, Matyas D J, Crocker C, Dungan K A, Matola B R and Rohlen J 2014 *Phys. Rev. Lett.* **113** 063001
[5] Walter C W, Gibson N D, Janczak C M, Starr K A, Snedden A P, Field R L and Andersson P 2007 *Phys. Rev. A* **76** 052702
[6] Walter C W, Gibson N D, Li Y G, Matyas D J, Alton R M, Lou S E, Field R L, Hanstorp D, Pan L and Beck D R 2011 *Phys. Rev. A* **84** 032514
[7] Bilodeau R C and Haugen H K 2000 *Phys. Rev. Lett.* **85** 534
[8] Fischer A, Canali C, Warring U, Kellerbauer A and Fritzsche S 2010 *Phys. Rev. Lett.* **104** 073004
[9] Tang R L, Si R, Fei Z J, Fu X X, Lu Y Z, Brage T, Liu H T, Chen C Y and Ning C G 2019 *Phys. Rev. Lett.* **123** 203002
[10] O'Malley S M and Beck D R 2009 *Phys. Rev. A* **80** 032514
[11] Kellerbauer A and Walz J 2006 *New J. Phys.* **8** 45
[12] Yzombard P, Hamamda M, Gerber S, Doser M and Comparat D 2015 *Phys. Rev. Lett.* **114** 213001
[13] Cerchiari G, Kellerbauer A, Safronova M S, Safronova U I and Yzombard P 2018 *Phys. Rev. Lett.* **120** 133205
[14] Jordan E, Cerchiari G, Fritzsche S and Kellerbauer A 2015 *Phys. Rev. Lett.* **115** 113001
[15] Sidorov V A, Nicklas M, Pagliuso P G, Sarrao J L, Bang Y, Balatsky A V and Thompson J D 2002 *Phys. Rev. Lett.* **89** 157004
[16] Si Q, Rabello S, Ingersent K and Smith J L 2001 *Nature* **413** 804
[17] Hegger H, Petrovic C, Moshopoulou E G, Hundley M F, Sarrao J L, Fisk Z and Thompson J D 2000 *Phys. Rev. Lett.* **84** 4986
[18] Harrison N, Alver U, Goodrich R G, Vekhter I, Sarrao J L, Pagliuso P G, Moreno N O, Balicas L, Fisk Z, Hall D, Macaluso R T and Chan J Y 2004 *Phys. Rev. Lett.* **93** 186405
[19] Gu C, Jin R, Zeng D L, Yue X F, Gao X and Li J M 2016 *Chin. Phys. Lett.* **33** 043201
[20] Han H L, Zhang X Z and Shi T Y 2007 *Chin. Phys. Lett.* **24** 3392
[21] Yang X Y, Xu H F and Yan B 2019 *Chin. Phys. B* **28** 013203
[22] Peterson K A and Dyall K G 2015 *Computational Methods in Lanthanide and Actinide Chemistry*, edited by Dolg M (Chichester: John Wiley and Sons)
[23] Dinov K, Beck D R and Datta D 1994 *Phys. Rev. A* **50** 1144
[24] O'Malley S M and Beck D R 2000 *Phys. Rev. A* **61** 034501
[25] Berkovits D, Ghelberg S, Heber O and Paul M 1997 *Nucl. Instrum. Methods Phys. Res. B* **123** 515
[26] Davis V T and Thompson J S 2002 *Phys. Rev. Lett.* **88** 073003
[27] Cao X Y and Dolg M 2004 *Phys. Rev. A* **69** 042508
[28] O'Malley S M and Beck D R 2006 *Phys. Rev. A* **74** 042509
[29] Felfli Z, Msezane A Z and Sokolovski D 2009 *Phys. Rev. A* **79** 012714
[30] Felton J, Ray M and Jarrold C C 2014 *Phys. Rev. A* **89** 033407
[31] Tang R L, Fu X X, Lu Y Z and Ning C G 2020 *J. Chem. Phys.* **152** 114303
[32] Pelaez R J, Blondel C Delsart C and Drag C 2009 *J. Phys. B: At. Mol. Opt. Phys.* **42** 125001
[33] Carette T, Drag C, Scharf O, Blondel C, Delsart C Froese Fischer C and Godefroid M 2010 *Phys. Rev. A* **81** 042522
[34] Tang R L, Chen X L, Fu X X, Wang H and Ning C G 2018 *Phys. Rev. A* **98** 020501(R)
[35] Chen X L and Ning C G 2017 *J. Phys. Chem. Lett.* **8** 2735
[36] Luo Z H, Chen X L, Li J M and Ning C G 2016 *Phys. Rev. A* **93** 020501(R)
[37] Fu X X, Luo Z H, Chen X L, Li J M and Ning C G 2016 *J. Chem. Phys.* **145** 164307
[38] Fu X X, Tang R L, Lu Y Z and Ning C G 2019 *Chin. J. Chem. Phys.* **32** 187
[39] Fu X X, Lu Y Z, Tang R L and Ning C G 2020 *Phys. Rev. A* **101** 022502
[40] Tang R L, Fu X X and Ning C G 2018 *J. Chem. Phys.* **149** 134304
[41] Wiley W C and McLaren I H 1955 *Rev. Sci. Instrum.* **26** 1150
[42] Eppink A T J B and Parker D H 1997 *Rev. Sci. Instrum.* **68** 3477
[43] León I, Yang Z, Liu H T and Wang L S 2014 *Rev. Sci. Instrum.* **85** 083106
[44] Dick B 2014 *Phys. Chem. Chem. Phys.* **16** 570
[45] Tang R L, Fu X X, Lu Y Z and Ning C G 2019 *J. Phys. Chem. Lett.* **10** 702
[46] Sansonetti J E and Martin W C 2005 *J. Phys. Chem. Ref. Data* **34** 1559
[47] Kramida A 2011 *Comput. Phys. Commun.* **182** 419
[48] Peláez R J, Blondel C, Vandevraye M, Drag C and Delsart C 2011 *J. Phys. B: At. Mol. Opt. Phys.* **44** 195009
[49] Radziemski L J, Fisher K J, Steinhaus D W and Goldman A S 1972 *Comput. Phys. Commun.* **3** 9
[50] Tiesinga E, Mohr P J, Newell D B and Taylor B N 2019 *The 2018CODATA Recommended Values Fundamental Phys. Constants (Web Version* 8.0). Database developed by Baker J, Douma M and Kotochigova S. Available at http://physics.nist.gov/constants, National Institute of Standards and Technology Gaithersburg MD 20899